PCCP

Interfacial Solvation and Slow Transport of Hydrated Excess Protons in Non-ionic Reverse Micelles

SCHOLARONE™
Manuscripts

ARTICLE

Interfacial Solvation and Slow Transport of Hydrated Excess Protons in Non-ionic Reverse Micelles

Zhefu Li and Gregory A. Voth*[a]

This work employs molecular dynamics simulations to investigate the solvation and transport properties of hydrated excess protons (with a hydronium-like core structure) in non-ionic Igepal CO-520 reverse micelles of various sizes in a non-polar solvent. Multiscale Reactive Molecular Dynamics (MS-RMD) simulations were used to describe vehicular and hopping diffusion during the proton transport process. As detailed herein, an excess proton shows a marked tendency to localize in the interfacial region of micellar water pools. Slow proton transport was observed which becomes faster with increasing micellar size. Further analysis reveals that the slow diffusion of an excess proton is a combined result of slow water diffusion and the low proton hopping rate. This study also confirms that a low proton hopping rate in reverse micelles stems from the interfacial solvation of hydrated excess protons and the immobilization of interfacial water. The low water density in the interfacial region makes it difficult to form a complete hydrogen bond network near the hydrated excess proton, and therefore locks in the orientation of hydrated proton cations. The immobilization of the interfacial water also slows the relaxation of the overall hydrogen bond network.

1. Introduction

Proton transport (PT) in confined regions occurs in systems ranging from proton exchange membranes[1-5] to various biological systems (see, e.g., Refs[6-8]) Our previous studies on interfacial hydrated excess protons[9-13] predict that the PT process is significantly different in interfacial systems compared to how it behaves in the bulk. An interfacial preference for the hydrated excess proton (hydronium-like cation) was predicted as early as 2004.[9] Our prior study of lipid bilayer interfaces[12] also revealed that excess protons tend to form a distorted Zundel cation in the interfacial region. In a related study, Wolf *et al*.[14] also modeled that excess protons exhibit interface affinity near the DMPC membrane. Moreover, Zhang *et al.*[15] found from ab initio MD simulation that a hydrated excess proton tends to locate near an apolar hydrophobic interface, consistent with our earlier predictions.[9-12] These findings point to the importance of understanding the behavior and interfacial effects of hydrated protons in confined and interfacial systems.

Reverse micelles are amphiphilic structures that spontaneously form when surfactants are dissolved into non-polar solvents. A nanoscale water pool forms, which is surrounded by the hydrophilic head groups of the surfactant molecules. This resulting confinement alters both the structural and dynamical properties of the water pool compared to more conventional (e.g., bulk) systems. The thermodynamic and spectroscopic properties of reverse micelle systems have been studied with a variety of experimental techniques, including IR and Raman spectroscopy,[16, 17] NMR,[18] fluorescence probe,[19, 20]

etc. These efforts help to reveal the microscopic details of the confined water pool in a reverse micelle, which is usually portrayed as a roughly spherical shape that can be divided into two regions: (1) the interfacial region, in which both rotational and translational motions of water molecules are known to be largely immobilized; and (2) the central region, where the confinement effect is less severe and water molecules behave somewhat similar to the bulk system. However, the existence and nature of both regions depends on the size of the micellar water pool under consideration. In cases where the micellar water pools size is relatively small, the central region can be incomplete or even absent; in such instances all water molecules in the pool exhibit interfacial traits.

Recent work by Van der Loop et al.[21] applied GHz dielectric relaxation spectroscopy to non-ionic reverse micelle systems, which has provided further experimental evidence of the altered PT behavior in reverse micelles. They attributed this phenomenon to a collective slowing down of water dynamics. Earlier theoretical studies on reverse micelles[22, 23] and nanometer-scale water droplets[24] suggest that the interfacial solvation of the hydrated excess proton is responsible for slow proton diffusion. Based on what is already known about the interfacial affinity of excess proton,[9, 12, 14, 15] our present study was designed to examine the behavior of PT in reverse micelles with neutral head groups. More specifically, we investigated the solvation and transport of hydrated excess proton dissolved in micellar water pools of various sizes encapsulated by non-ionic surfactant molecules.

The paper is organized as follows: Section 2 describes the methods we used in our simulations, as well as details about our simulation system setup. Section 3 describes our findings about the equilibrium structure of reverse micelles, micellar solvation

[a.] Department of Chemistry, Chicago Center for Theoretical Chemistry, James Franck Institute, and Institute for Biophysical Dynamics, The University of Chicago, 5735 South Ellis Avenue, Chicago, Illinois 60637, United States

of the excess protons, and slow proton transport of those micellar excess proton. The paper concludes with a discussion of the analysis we employed to understand the slow transport of hydrated excess proton, a review of our findings, and closing observations.

2. Methodology

2.1 Multiscale Reactive Molecular Dynamics

The process of proton transport involves two mechanisms: vehicular transport and Grotthuss shuttling. The Grotthuss shuttling mechanism for PT involves the rearrangement of both hydrogen bonds and covalent bonds of water molecules and hydronium cations. Accordingly, any computational investigation into PT should accurately capture the breaking and formation of chemical bonds. Because traditional molecular dynamics (MD) methods rely on a static bonding topology, they are not capable of capturing one of the most important fundamental physical properties of PT, i.e., that of Grotthuss shutting. On the other hand, *ab initio* molecular dynamics (AIMD) can account for the electronic degree of freedoms to more fully describe dynamic bonding topology; however, this method is highly demanding computationally and proves to be prohibitively expensive for studying larger systems such as the reverse micelles of interest in the present work. In contrast, our work here and elsewhere utilized the Multiscale Reactive Molecular Dynamics (MS-RMD) method, and the very similar but more empirical Multistate Empirical Valence Bond (MS-EVB) method before it – which are both capable of capturing the Grotthuss mechanism – have been shown to accurately describe PT in various systems including reverse micelles,[23] proton exchange membranes and water interfaces[3, 4] and proteins (see, e.g., Ref. [8] for an example).

In the MS-RMD framework, the bonding topology of reactive species within a certain system is not fixed. Rather, the instantaneous ground state of a system $|\Psi\rangle$ is a linear combination of basis states $|i\rangle$. Each $|i\rangle$ represents a possible bonding topology of the system, such that

$$|\Psi\rangle = \sum_{i=1}^{N} c_i |i\rangle \tag{1}$$

where N is the total number of basis states, and c_i is the weight coefficient of the state. The coefficients are found by diagonalizing the quantum-like Hamiltonian at every MD timestep:

$$\boldsymbol{H}\boldsymbol{c} = E_0 \boldsymbol{c} \tag{2}$$

in which E_0 is the lowest eigenvalue corresponding to the ground-state of the system. The matrix elements of the Hamiltonian are defined as:

$$h_{ij} = \langle i|\boldsymbol{H}|j\rangle \tag{3}$$

The eigenvector is normalized so that:

$$\sum_{i=1}^{N} c_i^2 = 1 \tag{4}$$

With Hellmann-Feynman theorem, the force on each atom with every nuclei configuration can be calculated as:

$$F_i = -\left\langle \Psi_0 \left| \frac{\partial \boldsymbol{H}}{\partial \boldsymbol{x_i}} \right| \Psi_0 \right\rangle = -\sum_{m,n} c_m c_n \frac{\partial h_{mn}}{\partial \boldsymbol{x_i}} \tag{5}$$

This framework allows for charge delocalization and dynamic bonding topology rearrangement. As discussed herein, we have applied the new MS-RMD5 model,[25] which was developed via experiment-directed simulation (EDS) with AIMD. MS-RMD5 employs an anharmonic water model[26] that has a lower internal proton transfer barrier, therefore providing a higher proton self-diffusion constant that is closer to experimental values for bulk water. This latter feature represents an important PT property to determine via MS-RMD.

2.2 Simulation Details

Igepal CO-520 surfactant was used to construct the reverse micelles, which contain ether and hydroxyl oxygen atoms in their hydrophilic head groups. Hereafter, the hydroxyl group oxygen will be referred to as OHyx and ether oxygen atoms as OEther. The structure of the surfactant is shown in Figure 1. The pK_b of the head group in Igepal surfactants is found to be ~16 to 18, making it unlikely for the excess proton to protonate the head group. Further, based on experimental results[27, 28] and earlier simulations of methanol-water mixtures,[29] the presence of protonated alcohol oxygen is negligible compared to hydronium cations (H_3O^+) and therefore can be safely disregarded.
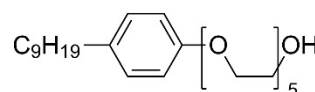
Figure 1. Structure of Igepal CO-520 surfactant molecule. Note that oxygen atoms in the hydroxyl group will be referred to as OHyx; and ether oxygen atoms will be referred to as OEther.

Reverse micelles of four sizes were constructed corresponding to the diameters of the water pool: 1nm, 2nm, 4nm, and 6nm. Experimentally, a ratio w_0 = [H₂O]/[surfactant] is generally used to provide an estimate of the size of the water pool in the reverse micelles. In our setup, the number of water molecules in each system was determined with the desired volume of the water pool and bulk water density at 298K. The number of surfactant molecules encapsulating the water pool was initially estimated from w_0 and then adjusted by examining the trajectories from classical MD simulations. The remainder of the simulation box was filled with cyclohexane molecules at a bulk density of 298K. Detailed compositions and final w_0 values for the reverse micelle systems can be found in Table 1. We defined the initial configurations of each system using the PACKMOL[30] software package. The general Amber force field (GAFF)[31] was used to describe cyclohexane and surfactant molecules with RESP charges obtained via *ab initio* calculations carried out by R.E.D. server.[32-35] The LAMMPS MD software[36] and an anharmonic water model aSPC/Fw[26] were utilized for all simulations. Detailed force-field parameters can be found in the Supporting Information. The reverse micelles were first equilibrated with classical MD simulation for 5 ns in the

constant *NPT* ensemble at 298K and 1 atm, and then another 5 ns in the constant *NVT* ensemble at 298K. Then, the water molecule closest to the center of mass (COM) of the water pool was replaced with a hydronium cation and a chloride anion, after which MS-RMD was applied in the NVE ensemble. For each micellar size, 5 statistically independent simulations were conducted, which resulted in a total of 15 ns of trajectories.

Table 1. Compositions of Reverse Micelle Systems

Water Pool Diameter	Number of H2O	Number of Surfactant	w0
1nm	15	15	1.0
2nm	118	52	2.3
4nm	994	208	4.8
6nm	3186	468	6.8

3. Results and Discussion

3.1 Equilibrium Structure of Reverse Micelles

We first looked at specific intrinsic structural properties of these confined environments, which we surmised may impact the solvation of the excess proton charge. Recall that a reverse micelle represents an inhomogeneous environment, with a water pool surrounded by the hydrophilic head groups of surfactant molecules. For this inhomogeneous system, we applied a local density profile function to describe how the density varied as a function of distance from a reference point. With the center of mass of the water pool as the reference point, the local density of a species was defined as:[23]
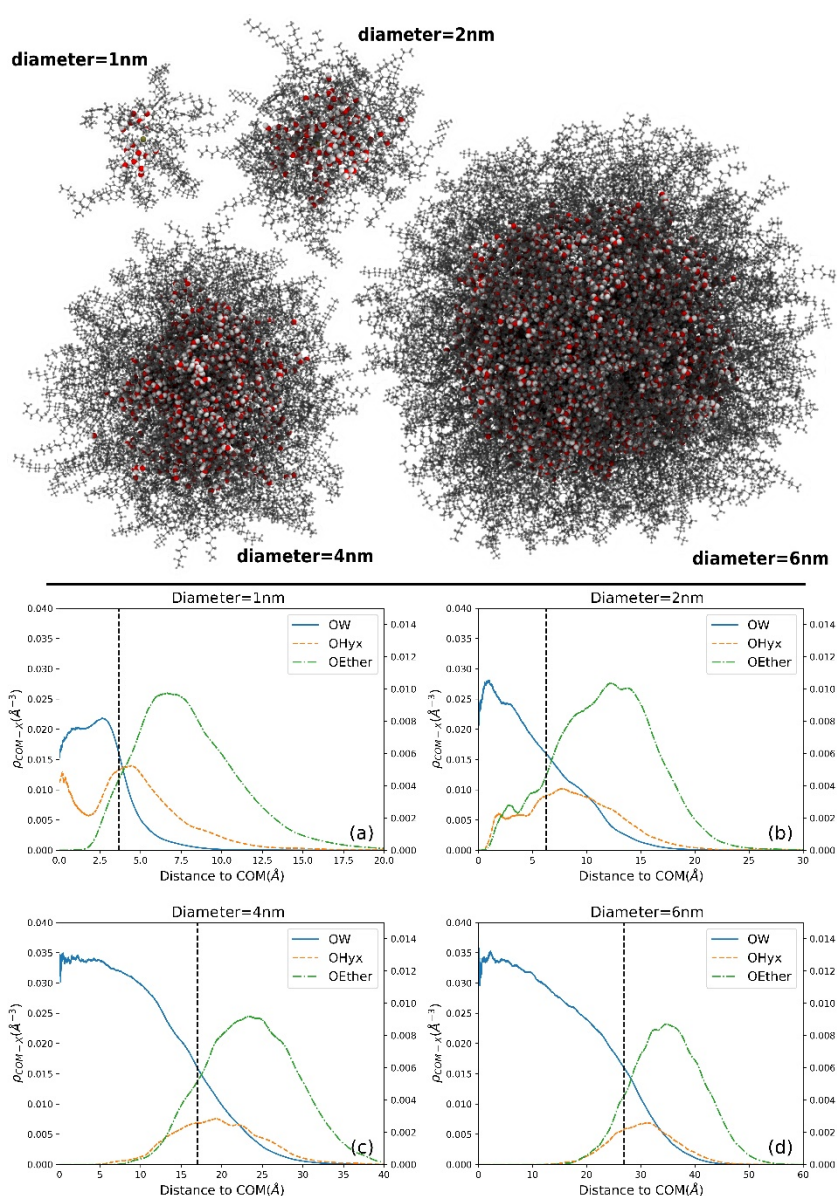
Figure 2. Top Panel: Snapshots of reverse micelles of simulated diameters. Lower Panel: Local density profiles with COM of water pool as center of different micellar sizes: (a) diameter=1nm, (b) d=2nm, (c) d=4nm, and (d) d=6nm. OW: oxygen atom water molecule; OHyx: hydroxyl oxygen in surfactant head group; OEther: ether oxygen in surfactant head group
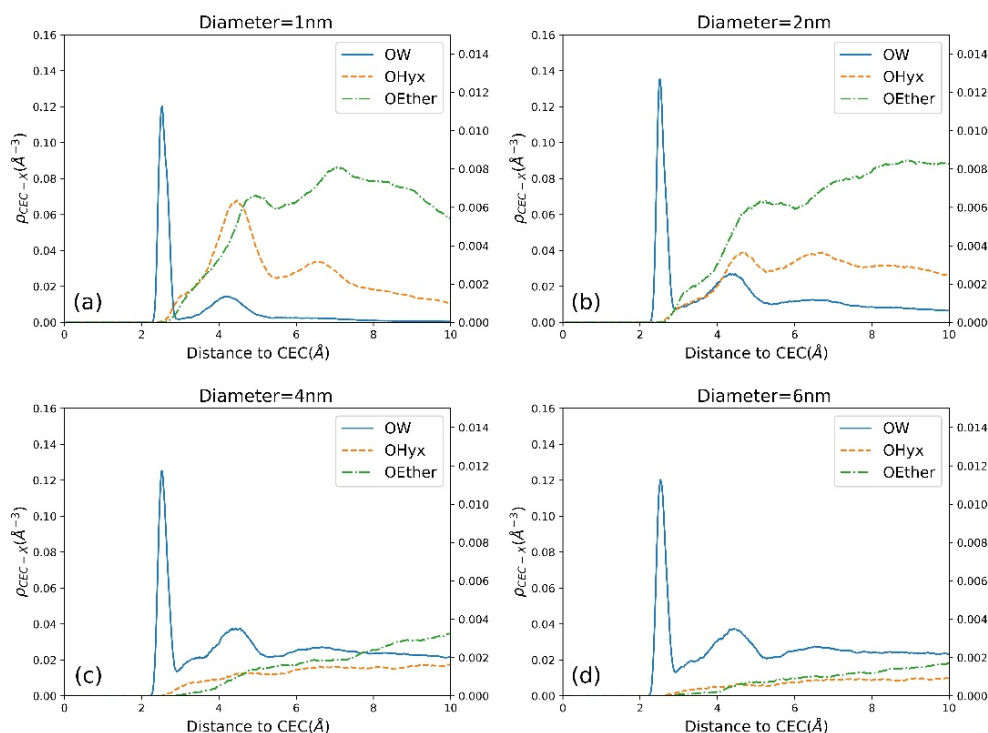
Figure 3. Local density profiles with pivot oxygen (O*) as center of different micellar sizes: (a) diameter=1nm, (b) d=2nm, (c) d=4nm and (d) d=6nm. OW: oxygen atom water molecule, OHyx: hydroxyl oxygen in surfactant head group, OEther: ether oxygen in surfactant head group

$$\rho_{COM-\alpha} = \frac{1}{4\pi r^2} \langle \sum_{i=1}^{N} \delta(|r_i^{\alpha} - R_{COM}| - r) \rangle \quad (6)$$

in which R_{COM} is the COM coordinate, r_i^{α} denotes the coordinate of site α on the i-th molecule. Figure 2 presents the local density profile of water oxygen (OW), OHyx, and OEther. Note that the OW plot uses the left y-axis and the surfactant atoms (OHyx and OEther) use the right y-axis. In each figure, the vertical black dashed line indicates the location of the Gibbs dividing surface (GDS), which represents an idealized, zero-volume plane to separate two phases. The GDS utilizes the local density of the target species and is defined as the surface where the local density is half of the bulk density. For this study, we decide the GDS locates at where local water density is 0.016 Å^{-3}, half of the number density of bulk water at 298K (0.032 Å^{-3}). For our reverse micelles, atoms in the surfactant hydrophilic head group (OHyx and OEther) both reached a significant local density at the GDS, which means the interface was a mixture of water molecules and surfactant head groups, which is important since the head groups can play a role in interfacial excess proton behavior.

For the two larger reverse micelles (d=4nm, d=6nm), we noted that the water local density near the COM of the water pool reached bulk water density, which indicates the presence of both a central bulk-like phase and an interfacial phase in these two larger reverse micelles. However, the density of water decreased quite rapidly with increasing distance from the COM. In the case of the two smaller reverse micelles (d=1nm, d=2nm), the central density did not reach bulk water density. Accordingly, the absence or incompleteness of a bulk region in a smaller micellar water pool may lead to structural and

dynamic differences of the water molecules, which could impact the behavior of excess proton.

3.2 Micellar Solvation of Hydrated Excess Protons

The hydrated excess proton is usually described as two limiting structures: a Zundel cation, $H_5O_2^+$, and the Eigen cation, $H_9O_4^+$. In bulk water, it has been proposed that the excess proton migrates through the hydrogen bond network from one water molecule to another, in an Eigen-Zundel-Eigen sequence. In confined systems such as reverse micelles, it is important to recognize the underlying impact of inhomogeneity, as well as the interfacial effect on the PT process. The relatively low water density near the interface is highly likely to impact the hydrogen
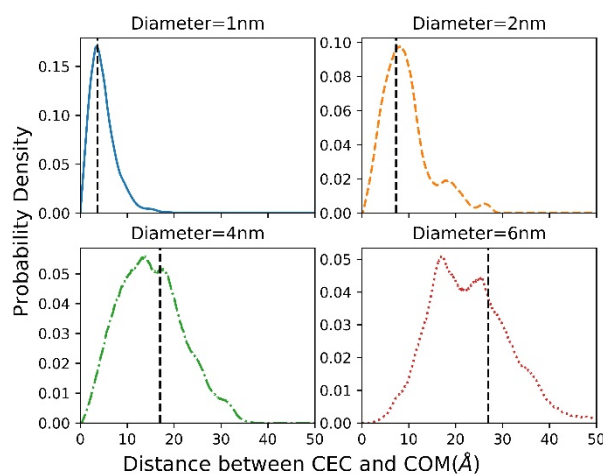
Figure 4. Probability density of hydrated excess proton CEC (y-axis) corresponding to the distance to COM (x-axis) in four reverse micelle systems. The dashed vertical line is the Gibbs Dividing Surface (GDS).
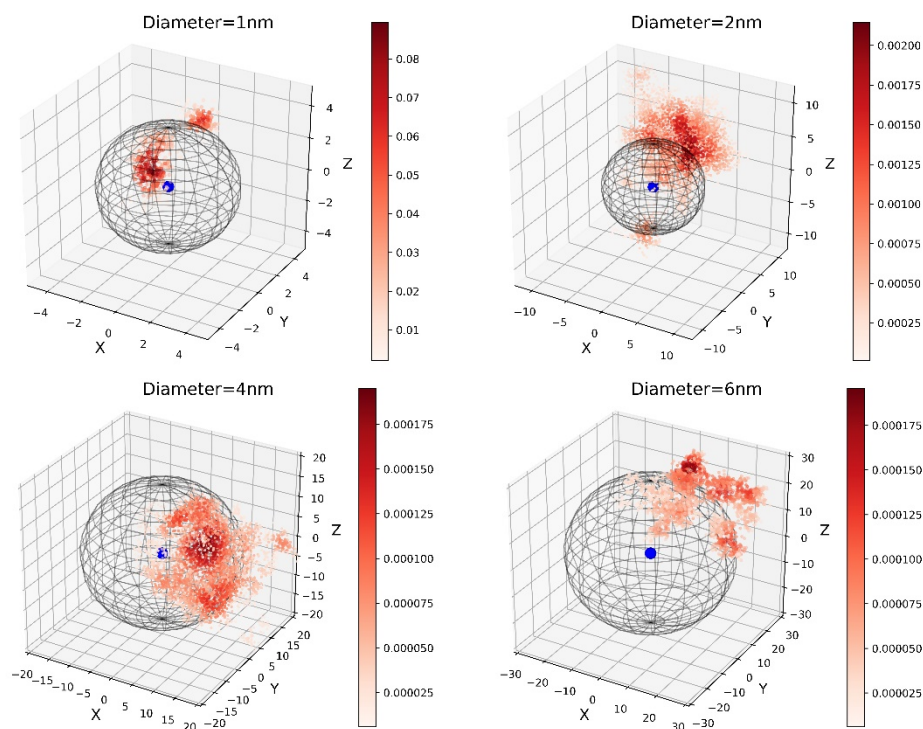
Figure 5. 3D visualization of CEC probability density over a 3-ns time period for all four reverse micelles systems: d= 1 nm, d= 2 nm, d= 4 nm, and d=6 nm. The hydrated excess proton CEC coordinates are relative to the COM, and are color-coded according to the local density of CEC across the entire time series. The blue dot denotes the origin (COM coordinate), and the black wireframe denotes the GDS.

bond network in the interfacial region, which in turn affects the PT process. In MS-RMD, the location of the excess protonic center of excess charge (CEC) can be defined by:

$$\boldsymbol{r}_{CEC} = \sum_{i=1}^{N} c_i^2 \, \boldsymbol{r}_{COC}^i \qquad (7)$$

in which $\boldsymbol{r}_{COC}^i$ is the center of charge of the hydronium cation in the i-th MS-RMD basis eigenstate. The eigenstate with the largest c_i is known as the "pivot" state, and the hydronium oxygen in such a state is known as the pivot oxygen (hereafter referred to O*). Figure 3 shows a density profile depicting the solvation structure of the hydrated excess proton cation with O* as the reference point. In all four reverse micelle systems, the OW plots present two peaks, representing the first and the second shell of the hydronium-like cation (the core of the hydrated excess proton structure). In Figure 3(a), the oxygen atoms in the surfactant head group (OHyx and OEther) contribute considerably to the formation of the second solvation shell. With increasing micellar water pool size, the contribution of the surfactant head group to the second solvation shell diminishes. Based on the data presented in Figures 2 and 3, there is a strong interaction between the hydronium-like cation core and the surfactant in the smaller reverse micelles, suggesting that the hydrated excess proton is located near the interface. As micellar size increases and the water pool becomes more bulk-like, the interaction between the hydronium and the surfactant molecules weakens.

To further verify the binding between the excess proton and the interface, we examined the probability density function (PDF) of the distance between the excess proton CEC and the COM of the water pool (see Figure 4). The colored lines in this

figure depict the PDF, while the vertical dashed lines depict the GDS of the micellar water pool. For all four reverse micelles, the PDF peak was observed to be more distant from the COM and nearer the GDS, indicating that the center of excess charge (i.e., the hydrated excess proton) has a tendency to move away from the center of the water pool and reside near the interface, even for non-ionic surfactants. With increasing micellar size, the PDF shows a wider distribution, with the peak moving left and away from the GDS, indicating a weaker binding between the hydrated excess proton and the interface.

Furthermore, Figure 5 provides a 3D visualization of CEC probability density for each system during one independent simulation run of 3 ns, where each data point is a CEC coordinate relative to COM at one time step and is color-coded according to the probability density of the CEC through the entire time series. The blue dot represents the COM and the black wireframe represents the GDS. As shown in Figure 5, the hydrated excess proton CEC density accumulates mostly away from the COM and near the interface radially, which is consistent with the results provided in Figure 4. The CEC also tends to be laterally trapped in a certain region of the interface, leaving much of the interfacial phase unvisited.

Based on results presented in Figures 4 and 5, we conclude that the excess proton in the reverse micelles is localized near the interfacial region, both radially and laterally. Moreover, the binding between the excess proton and the interface was found to decrease with increasing micellar diameter.

3.3 Proton Transport in Reverse Micelles

Having established the nature of micellar solvation of the hydrated excess protons, we then examined the underlying
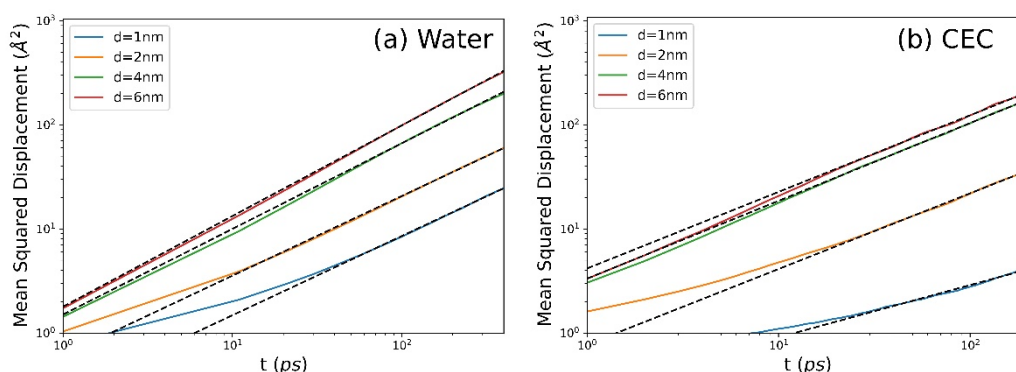
Figure 6. Mean squared displacement of oxygen in (a) water, and (b) hydrated excess proton CEC in four reverse micelle systems, plotted in log-log scale.

Figure 7. Forward excess proton hop function calculated from an MD trajectory from each reverse micelle system and a bulk water system.
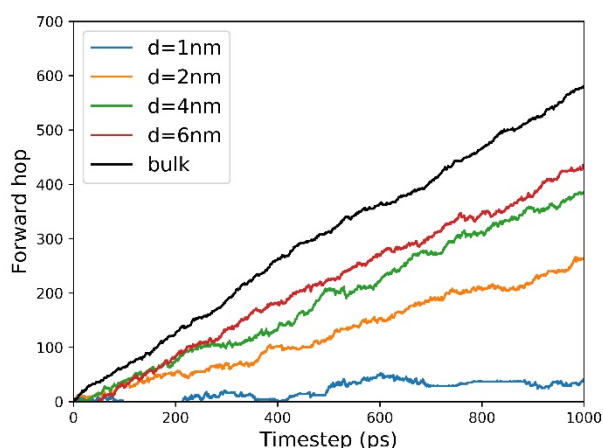
dynamical characteristics that contribute to the PT process in the reverse micelles. First, we calculated the diffusive behavior of the hydrated excess proton and the water molecules in reverse micelle. In bulk systems, the diffusion of a species can be described with the usual Einstein relation:

$$\langle r^2 \rangle_{t \to \infty} = 6Dt \tag{8}$$

in which D is the diffusion coefficient and $\langle r^2 \rangle$ is the mean squared displacement (MSD) of the species, assuming the origin of all trajectories is taken to be zero. The Einstein relation describes a linear relation between the MSD and time. However, in confined systems, there is often not a linear relation between the MSD and time, but instead a power-law relation (see., e.g., ref[37] for the case of proton exchange membranes):

$$\langle r^2 \rangle = 6D_\alpha t^\alpha \tag{9}$$

where $0 < \alpha < 1$ for sub-diffusivity. Note that the unit of D_α in equation (9) is different when α is different, making it problematic to compare D_α values in different systems. On the other hand, the α values is more indicative of nature of dynamics followed by water molecules and the CEC. Figure 6 depicts the MSD of water oxygen and the excess proton CEC in

each of the four reverse micelle systems. The parameters of sub-diffusivity (α and D_α) of water and CEC were obtained with least square fitting according to Equation (9) and shown in Tables 2. The micellar diffusion of water and excess proton shows to be slower compared to the bulk system. For our study, we observed a clear trend that with increasing water pool size, both the diffusivity of the water and hydrated excess proton CEC increased, as expected. The slowing down of the relaxation rate of water in reverse micelles has in fact been widely confirmed via various experimental approaches including pulsed NMR,[38] fluorescent spectroscopy,[39-41] dielectric measurements,[42, 43] as well as by computational approaches.[44, 45]

Table 2. Fitted parameters of sub-diffusivity for water oxygen and hydrated excess proton (CEC) in each reverse micelle

	d=1nm	d=2nm	d=4nm	d=6nm	bulk[25, 26]
α_{OW}	0.76	0.77	0.82	0.87	1.0
$D_{\alpha OW}$ (Å²/psᵅ)	0.042	0.10	0.25	0.30	0.23
α_{CEC}	0.50	0.73	0.74	0.74	1.0
$D_{\alpha CEC}$ (Å²/psᵅ)	0.047	0.13	0.55	0.69	0.47

The diffusion of excess proton represents the collective outcome of the vehicular motion of hydronium cations (H_3O^+) and the Grotthuss hopping of protons from one water molecule to another; accordingly, the vehicular motion of excess proton should be strongly correlated with the water diffusion. For instance, with increasing micellar diameter and reduced effective interaction between the excess proton and the interface, the diffusion of the excess proton increases. Slow diffusion of interfacial water slows the diffusion of the excess proton once it reaches the interface and helps to trap the proton. Moreover, it has been shown that the rearrangement of the hydrogen bond network as a whole plays a key role in long-range structural diffusion,[46, 47] which in turn is correlated with water diffusion. The simultaneous slowing down of the diffusive motion of water molecules and the hydrated proton CEC is consistent with the correlation mentioned above.

It is also valuable to evaluate the rate of proton hopping in reverse micelles. Using the MS-RMD framework, proton hopping events can be identified by observing the identity

ARTICLE
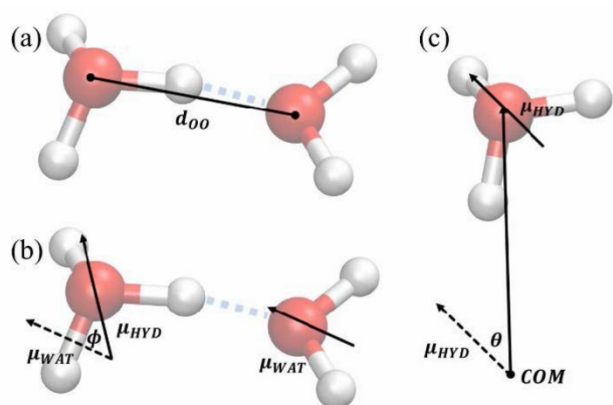
Figure 8. Three characteristics used to describe the structure of the hydronium-like complex. (a) d_{OO}, the distance between the two oxygen atoms; (b) ϕ, the angle between the dipole moment of the hydronium cation and water molecule; (c) θ, the angle between the dipole moment of the hydronium cation and its relative coordinate vector to the COM of the water pool.

change of the pivot hydronium in the dynamic algorithm. Specifically, two types of proton hopping can be observed: (1) oscillatory shuttling, during which the excess proton hops back and forth between the pivot hydronium cation and a water molecule in its first solvation shell; and (2) Grotthuss shuttling, during which the proton hops first and then on to a third water molecule instead of hopping back to its donor. It is clear that Grotthuss shuttling should be considered as the primary contributor to the mobility of the excess proton. Accordingly, we utilized a "forward hop" accumulation function to evaluate the rate of Grotthuss shuttling. The forward hop equation is given as:

$$h(t) = h(t-1) + \delta h(t)$$

$$h(0) = 0 \tag{10}$$

in which t is the time step, h is the accumulated hopping. The increment $\delta h(t)$ is 0 if there is no proton hop, 1 if the proton hops to a new receptor, and -1 if it hops back to the previous donor. To clarify the definition of "previous donor", we consider a scenario in which the pivot hydronium identity follows this sequence: 1-2-3-2-3. The $\delta h(t)$ for each step will be +1, +1, -1, +1, which is based on the fact that when the proton hops from 3 back to 2, the "previous donor" of water 2 becomes water 1 again. This function distinguishes the aforementioned two shuttling events. This type of accumulation function measures the topological distance between hydronium at time 0 and at time t in terms of the number of proton hops.

Figure 7 depicts the forward proton hop function for each of the four reverse micelle systems and the bulk water system. In a water pool as small as 1nm in diameter, there is no bulk-like region in the pool, and all water molecules are interfacial. Moreover, the almost flat forward hop function indicates that the interfacial environment has greatly impeded the proton hopping. With increasing micellar size, however, the proton hopping rate increases accordingly. Keeping in mind that the solvation environment of the excess proton becomes more bulk-like with increasing micellar size, Figure 7 provides direct evidence of the low proton hopping rate of the interfacial excess protons. Both proton transport components—the vehicular motion of the hydronium cation and Grotthuss proton
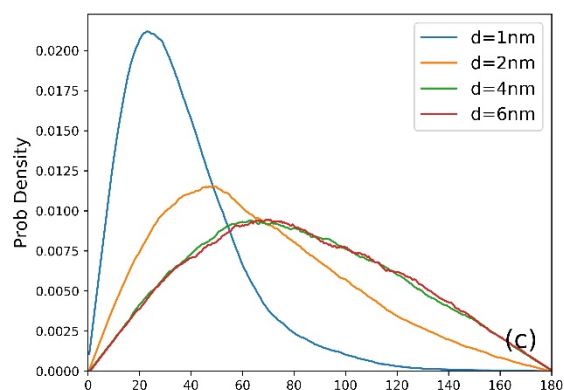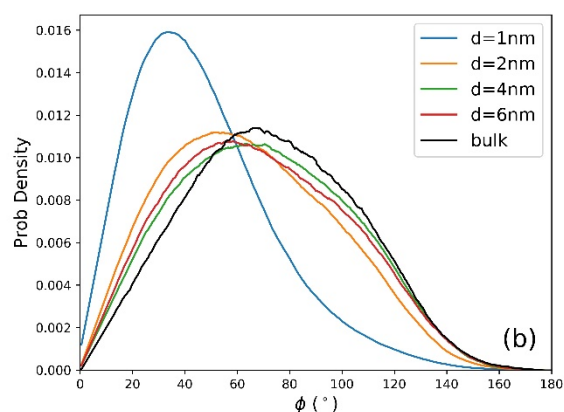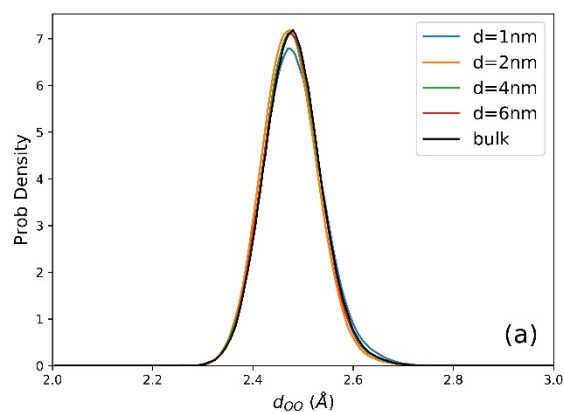
Figure 9. Probability density of characteristics for structural properties of hydronium-like complexes. (a) d_{OO} of reverse micelles and bulk system; (b) φ of reverse micelles and bulk system; (c) θ of reverse micelles.

hopping—clearly become slower in reverse micelle systems, as a result of the slow PT near the interface which makes it difficult for hydrated excess protons to move back to bulk-like regions once they reach the interface. This explanation for the slowed hydrated proton diffusion differs from that of Van der Loop et al.,[21] who assumed the excess proton would not be at the interface.

3.4 Discussion on Slow Micellar Proton Hopping

In this section, we add additional insight to the low proton hopping rate in reverse micelles. One possible factor for this behavior is the difference in the structural properties of the hydronium-like complex. To define a hydronium complex, one must first locate the pivot or "core" hydronium cation. For every

water molecule in its first solvation shell, δ as defined in Equation (11) is calculated as:

$$\delta = |d_{O^*H} - d_{O_WH}| \tag{11}$$

in which d_{O^*H} is the distance between the shared hydrogen atom and the hydronium oxygen, and d_{O_WH} is the distance between the shared hydrogen atom and the water oxygen. The water molecule with the minimal δ was identified as the "special pair" of the hydronium cation. Between the hydronium cation and its "special pair", a Zundel-like complex could be identified. We then introduced two characteristics to describe the structural properties of such hydronium-like complexes: (1) d_{OO}, the distance between the two oxygen atoms, and (2) ϕ, the angle between the dipole moment of the hydronium cation (μ_{HYD}) and the dipole moment of water molecule (μ_{WAT}). Both d_{OO} and ϕ represent inherent structural properties of the hydronium complex. We also defined θ as the angle between the dipole moment of the hydronium cation and its relative coordinate vector to the COM of the water pool. The angle θ is an external property that describes the orientation relationship between the hydronium cation and the interface. A small θ means the dipole moment of the hydronium cation is pointing radially outwards from the water pool and perpendicular to the interface; therefore, a θ close to 90° indicates that the dipole moment is parallel to the interface, while a θ close to 180° indicates that it points radially inwards toward the water pool. These characteristics are illustrated in Figure 8.

For each reverse micelle system, the probability density distribution for every characteristic described above was calculated from the simulation trajectories. In Figure 9, the results from the four reverse micelle systems are depicted and compared with corresponding data from the bulk system (if applicable). First, we observed only minor differences in d_{OO} between the d=1nm micelle and the remaining systems, as shown in Figure 9(a). Second, a relatively larger distortion regarding the angle between two dipole moments was observed, as indicated in Figure 9(b). Specifically, in the d=1nm reverse micelle, the average angle between the dipole moments was significantly smaller than that of the bulk system. The structural distortion of hydronium complexes in smaller micellar water pools may be a result of low water density in the interfacial region, as well as the participation of surfactant head groups in the solvation shells of the hydronium. It is possible that the slightly distorted structure of the hydronium complex interrupts the local hydrogen bond (HB) network near the excess proton and hinders the PT process in smaller reverse micelles.

Next, as shown in Figure 9(c), we observed that θ is a rather distinct structural property across the four reverse micelle systems. With increasing micellar size, the mode of the probability density distribution of θ increased, with the distribution widening. This finding indicates that (1) the orientation of the hydronium dipole moment evolves from radial to lateral, and (2) re-orientation becomes relatively free with increasing micellar size. It should also be noted that a locked re-arrangement of the hydronium dipole exerted a

negative impact on the delocalization of the excess proton and hindered the relaxation of the hydrogen bonds nearby.

Furthermore, it is likely that low interfacial water density and the participation of non-reactive surfactant head groups in the solvation environment of the hydronium-like cation slowed down proton hopping. As discussed in an earlier section of this paper, the excess proton resides in the interfacial region of the micellar water pool where the water density is lower and is mixed with surfactant head groups. The difficulty for the hydronium cation to locate water molecules and form a complete HB network hinders the excess proton from hopping. The low interfacial water density may also contribute to the locked dipole orientation of the hydronium cation, which can be attributed to a difficulty in breaking an existing HB network to form a new one.

We next investigated the overall dynamics of the HB network of all water molecules in micellar water pools. In this report, the hydrogen bonds are identified according to specific geometric criteria: a hydrogen bond is recognized when the distance between donor oxygen and acceptor oxygen is within 3.0 Å and the O-H-O angle is between 160° and 180°. Accordingly, we used a time correlation function[48] to evaluate the relaxation time of the hydrogen bonds:

$$C_{HB}(t) = \frac{\langle h(0) \cdot h(t) \rangle}{\langle h \rangle} \tag{12}$$

in which $h(t)$ is 1 if the tagged hydrogen bond exists at time t and 0 if it does not. The $\langle ... \rangle$ symbol denotes averaging over all atom pairs feasible for hydrogen bonding and over the entire simulation trajectory. This correlation function $C_{HB}(t)$ describes the probability that a certain HB remains intact after a certain amount of time t, disregarding possible HB breakage during interim times. The associated relaxation time of the $C_{HB}(t)$ function describes the structural relaxation of the hydrogen bond network. The autocorrelation of HBs in the bulk system can be fit with an exponential decay:[49]

$$C_{HB}(t) = a \exp\left(-\frac{t}{\tau}\right) \tag{13}$$

However, the micellar HB autocorrelation functions are clearly not exponential and can be very well fit with a bi-exponential decay such that:

$$C_{HB}(t) = a_1 \exp\left(-\frac{t}{\tau_1}\right) + a_2 \exp(-\frac{t}{\tau_2}) \tag{14}$$

in which $\tau_1 < \tau_2$. The bi-exponential decay behavior of hydrogen bonding in micellar water pools indicates that there was a second process proceeding simultaneously alongside the normal structural relaxation of the HB network. The results of $C_{HB}(t)$ and the fitted plots for the four reverse micelle systems and bulk water system are shown in Figure 10. The fitted parameters are listed in Table 3.

Table 3. Parameters of the exponential/bi-exponential decay of $C_{HB}(t)$ in the reverse micelles and bulk systems

	a_1	$\tau_1(ps)$	a_2	$\tau_2(ps)$
d=1nm	0.12	29.1	0.61	485.9
d=2nm	0.30	23.9	0.23	134.7
d=4nm	0.36	8.1	0.12	84.5
d=6nm	0.38	6.9	0.09	78.1
bulk (MS-RMD5)	0.43	3.78	-	-

We note that the τ values we obtained for the bulk system are comparable with previous results.[50] For the four reverse micelle systems investigated in this study, it should also be noted that with increasing micellar size, both τ_1 and τ_2 decreased accordingly, indicating a faster relaxation for both processes, as expected. Thus, we assume that the shorter τ_1 represents a short-range relaxation process of the HB, while the longer τ_2 correlates to the long-range micellar diffusion of HB
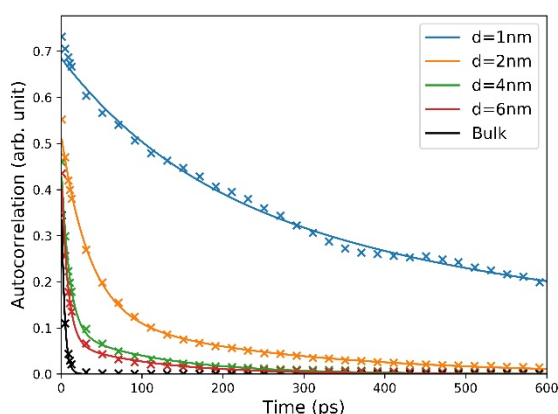
Figure 10. $C_{HB}(t)$ of d=1nm, d=2nm, d=4nm and d=6nm reverse micelle systems and bulk system. Original simulation results are indicated by crosses, and fitted bi-exponential figures are depicted as solid lines.

pairs (i.e., water molecules and hydronium-like hydrated proton cations). The size effects of short-range HB relaxation can be attributed to the slow relaxation of micellar water. With increasing micellar size, the water pool becomes more bulk-like and the rate of water relaxation intensifies. As a result, the short-range relaxation of HB also increases. Conversely, we assume that the size effect of long-range HB relaxation is a result of slow micellar water diffusion, as described in Section 3.2 and shown in Figure 6(a). Spectroscopic research efforts conducted by Fayer et al.[51, 52] revealed similar size effect, relating the overall slower orientation relaxation in micellar water pools of smaller and intermediate sizes to the slow water dynamics of the interfacial water shell. In short, immobilized micellar interfacial water[38-45] slows the relaxation of hydrogen bonding, thus promoting its greater stability after a certain amount of time.

Conclusions

Non-ionic aqueous reverse micelles are valuable for studying confined aqueous systems. In this work, we performed MS-RMD simulations of one hydrated excess proton in non-ionic reverse

micelles of four varying sizes, with the goal of determining the general impact on the behavior of the excess proton posed by the confinement in these micelles. Our simulations present a microscopic analysis of micellar water pool behavior consistent with prior research efforts.[16-19] In our reverse micelles, the hydrated excess proton remains near the interface and also interacts with surfactant head groups, which participates in the formation of a second solvation shell. The hydrated excess proton is found to be localized both radially and laterally near the interface.

This investigation also confirmed that proton transport is slow in reverse micelles, which we ascribe to both the slow vehicular motion of hydronium-like cations and a lower proton Grotthuss hopping rate. The former tendency is also connected to the slow diffusion of interfacial water, which is consistent with previous theoretical[44, 45] and experimental[38-43] findings. To further elucidate the impact of the low proton hopping rate, we analyzed the structure of the hydronium-like complex. The resulting data confirmed that slow proton hopping occurs as a result of both the enhanced interfacial solvation of the excess hydrated proton and the immobilization of the interfacial water. Low water density in the interfacial region (i.e., where the hydrated excess proton resides) makes it difficult for an excess proton to form a complete HB network around it, thus hindering the proton hopping. Moreover, the orientation of the hydronium is locked because of the difficulty in rearranging the existing HB network and forming a new one. For the overall HB network, we observed a bi-exponential decay of the micellar HB autocorrelation function involving (a) short-range HB relaxation, and (b) long-range micellar solvation of HB pairs. The two relaxation times, τ_1 and τ_2, both showed a monotonic decreasing trend with increasing micellar size. In particular, we can attribute micellar water relaxation to the short-range τ_1, and micellar HB pair diffusion to the long-range τ_2. With increasing micellar size, the hydrated excess proton more easily leaves from the interface and the surrounding solvation environment becomes less interface-like and more bulk-like, thus decreasing the relaxation time for both processes.

In the future, it will be interesting to explore how other surfactants could impact confinement effects on proton transport. For instance, Rosenfeld and Schmuttenmaer[53] reported that the properties of a given surfactant will impact the hydrogen bond network among water molecules, which in turn may influence the PT process. Another potentially interesting direction for a future study would be to construct a set of reverse micelles with increasing diameter, such that the behavior of excess proton may eventually conforms to proton behavior in the bulk system. The downside of such an investigation is that it can be expensive and time-consuming to conduct all-atom molecular dynamics simulation on such large systems because of the large number of atoms in surfactants and solvent molecules. One possible way to overcome this hurdle is to construct coarse-grained (CG) reverse micelle systems using a recently developed "Ultra-CG" method in which the CG interactions are dependent on the local environment via "states" inside the CG sites.[54] As can be seen from a recent study examining their performance in complex interfacial systems,[55]

this Ultra-CG approach is expected to distinguish the different environments of micelle molecules and provide significantly more accurate structural correlations.

Conflicts of interest

There are no conflicts to declare.

Acknowledgements

Notes and references

1. A. Roy, M. A. Hickner, H.-S. Lee, A. Badami, X. Yu, Y. Li, T. Glass and J. E. McGrath, *ECS Transactions*, 2007, **2**, 45-54.
2. M. K. Petersen, A. J. Hatt and G. A. Voth, *The Journal of Physical Chemistry B*, 2008, **112**, 7754-7761.
3. C. Arntsen, J. Savage, Y. L. S. Tse and G. A. Voth, *Journal*, 2016, **16**, 695-703.
4. J. Savage and G. A. Voth, *Journal of Physical Chemistry C*, 2016, **120**, 3176-3186.
5. Z. Rao, C. Zheng and F. Geng, *Computational Materials Science*, 2018, **142**, 122-128.
6. D. M. Popović and A. A. Stuchebrukhov, *Journal of the American Chemical Society*, 2004, **126**, 1858-1871.
7. P. E. M. Siegbahn and M. R. A. Blomberg, *Journal of Physical Chemistry A*, 2008, **112**, 12772-12780.
8. R. Liang, J. M. J. Swanson, M. Wikström and G. A. Voth, *Proceedings of the National Academy of Sciences*, 2017, **114**, 5924-5929.
9. M. K. Petersen, S. S. Iyengar, T. J. F. Day and G. A. Voth, *Journal of Physical Chemistry B*, 2004, **108**, 14804-14806.
10. S. Iuchi, H. Chen, F. Paesani and G. A. Voth, *Journal of Physical Chemistry B*, 2009, **113**, 4017-4030.
11. H. Chen, J. Xu and G. A. Voth, *The Journal of Physical Chemistry B*, 2009, **113**, 7291-7297.
12. T. Yamashita and G. A. Voth, *Journal of Physical Chemistry B*, 2010, **114**, 592-603.
13. J. Savage, Y.-L. S. Tse and G. A. Voth, *The Journal of Physical Chemistry C*, 2014, **118**, 17436-17445.
14. M. G. Wolf, H. Grubmüller and G. Groenhof, *Biophysical Journal*, 2014, **107**, 76-87.
15. C. Zhang, D. G. Knyazev, Y. A. Vereshaga, E. Ippoliti, T. H. Nguyen, P. Carloni and P. Pohl, *Proceedings of the National Academy of Sciences*, 2012, **109**, 9744-9749.
16. A. D'Aprano, A. Lizzio, V. Turco Liveri, F. Aliotta, C. Vasi and P. Migliardo, *Journal of Physical Chemistry*, 1988, **92**, 4436-4439.
17. T. K. Jain, M. Varshney and A. Maitra, *Journal of Physical Chemistry*, 1989, **93**, 7409-7416.
18. H. Hauser, G. Haering, A. Pande and P. L. Luisi, *Journal of Physical Chemistry*, 1989, **93**, 7869-7876.
19. M. Belletête, M. Lachapelle and G. Durocher, *Journal of Physical Chemistry*, 1990, **94**, 5337-5341.
20. T. K. De and A. Maitra, *Advances in Colloid and Interface Science*, 1995, **59**, 95-193.
21. T. H. Van der Loop, N. Ottosson, T. Vad, W. F. C. Sager, H. J. Bakker and S. Woutersen, *Journal of Chemical Physics*, 2017, **146**, 131101.
22. M. H. H. Pomata, D. Laria, M. S. Skaf and M. D. Elola, *Journal of Chemical Physics*, 2008, **129**, 244503.
23. J. Rodriguez, J. Martí, E. Guàrdia and D. Laria, *Journal of Physical Chemistry B*, 2007, **111**, 4432-4439.
24. J. Rodriguez, D. Laria, E. Guàrdia and J. Martí, *Physical Chemistry Chemical Physics*, 2009, **11**, 1484-1490.
25. C. Arntsen, C. Chen and G. A. Voth, *Chemical Physics Letters*, 2017, **683**, 573-578.
26. K. Park, W. Lin and F. Paesani, *Journal of Physical Chemistry B*, 2012, **116**, 343-352.
27. T. G. Fillingim, N. Luo, J. Lee and G. W. Robinson, *Journal of Physical Chemistry*, 1990, **94**, 6368-6371.
28. L. S. Guss and I. M. Kolthoff, *Journal of the American Chemical Society*, 1940, **62**, 1494-1496.
29. M. K. Petersen and G. A. Voth, *Journal of Physical Chemistry B*, 2006, **110**, 7085-7089.
30. L. Martinez, R. Andrade, E. G. Birgin and J. M. Martínez, *Journal of Computational Chemistry*, 2009, **30**, 2157-2164.
31. J. Wang, W. Wang, P. A. Kollman and D. A. Case, *Journal of Molecular Graphics and Modelling*, 2006, **25**, 247-260.
32. C. I. Bayly, P. Cieplak, W. D. Cornell and P. A. Kollman, *Journal of Physical Chemistry*, 1993, **97**, 10269-10280.
33. F. Y. Dupradeau, A. Pigache, T. Zaffran, C. Savineau, R. Lelong, N. Grivel, D. Lelong, W. Rosanski and P. Cieplak, *Physical Chemistry Chemical Physics*, 2010, **12**, 7821-7839.
34. G. M. J. Frisch, W. Trucks, H. B. Schlegel, G. E. Scuseria, M. A. Robb, J. R. Cheeseman, G. Scalmani, V. Barone, B. Mennucci, G. A. Petersson, H. Nakatsuji, M. Caricato, X. Li, H. P. Hratchian, A. F. Izmaylov, J. Bloino, G. Zheng and J. L. Sonnenberg, *Gaussian 09, Revision D.01*, 2009, **1**, 1.
35. E. Vanquelef, S. Simon, G. Marquant, E. Garcia, G. Klimerak, J. C. Delepine, P. Cieplak and F. Y. Dupradeau, *Nucleic Acids Research*, 2011, **39**, W511-W517.
36. S. Plimpton, P. Crozier and A. Thompson, *Sandia National Laboratories*, 2007, **18**, 43.
37. J. Savage and G. A. Voth, *Journal of Physical Chemistry Letters*, 2014, **5**, 3037-3042.
38. D. W. Urry, S. Peng, J. Xu and D. T. McPherson, *Journal of the American Chemical Society*, 1997, **119**, 1161-1162.
39. N. E. Levinger, *Current Opinion in Colloid and Interface Science*, 2000, **5**, 118-124.
40. R. E. Riter, D. M. Willard and N. E. Levinger, *The Journal of Physical Chemistry B*, 1998, **102**, 2705-2714.
41. J. Zhang and F. V. Bright, *Journal of Physical Chemistry*, 1991, **95**, 7900-7907.
42. M. Fukuzaki, N. Miura, N. Shinyashiki, D. Kurita, S. Shioya, M. Haida and S. Mashimo, *Journal of Physical Chemistry*, 1995, **99**, 431-435.
43. E. H. Grant, V. E. R. McClean, N. R. V. Nightingale, R. J. Sheppard and M. J. Chapman, *Bioelectromagnetics*, 1986, **7**, 151-162.
44. R. J. Mashl, S. Joseph, N. R. Aluru and E. Jakobsson, *Nano Letters*, 2003, **3**, 589-592.

45.   S. Senapati and M. L. Berkowitz, *Journal of Chemical Physics*, 2003, **118**, 1937-1944.
46.   T. C. Berkelbach, H. S. Lee and M. E. Tuckerman, *Physical Review Letters*, 2009, **103**, 238302.
47.   H. Lapid, N. Agmon, M. K. Petersen and G. A. Voth, *Journal of Chemical Physics*, 2005, **122**, 014506.
48.   A. Luzar and D. Chandler, *Nature*, 1996, **379**, 55.
49.   A. Chandra, *Physical Review Letters*, 2000, **85**, 768.
50.   H. Xu, H. A. Stern and B. J. Berne, *Journal of Physical Chemistry B*, 2002, **106**, 2054-2060.
51.   D. E. Moilanen, E. E. Fenn, D. Wong and M. D. Fayer, *The Journal of chemical physics*, 2009, **131**, 014704.
52.   M. D. Fayer, *Accounts of chemical research*, 2011, **45**, 3-14.
53.   D. E. Rosenfeld and C. A. Schmuttenmaer, *Journal of Physical Chemistry B*, 2011, **115**, 1021-1031.
54.   J. F. Dama, J. Jin and G. A. Voth, *Journal of Chemical Theory and Computation*, 2017, **13**, 1010-1022.
55.   J. Jin and G. A. Voth, *Journal of Chemical Theory and Computation*, 2018, **14**, 2180-2197.
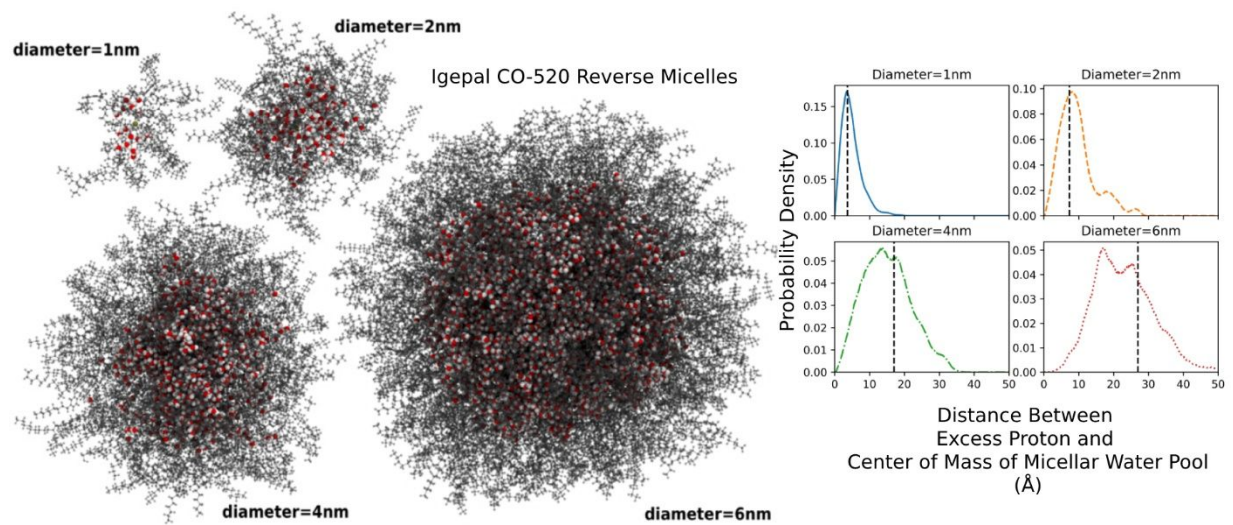
Simulations show that hydrated excess protons in non-ionic reverse micelles resides near the interface, contrary to some experimental assumptions.